iScience

CellPress
OPEN ACCESS

Article

# CXCR4-enriched T regulatory cells preferentially home to bone marrow and resolve inflammation

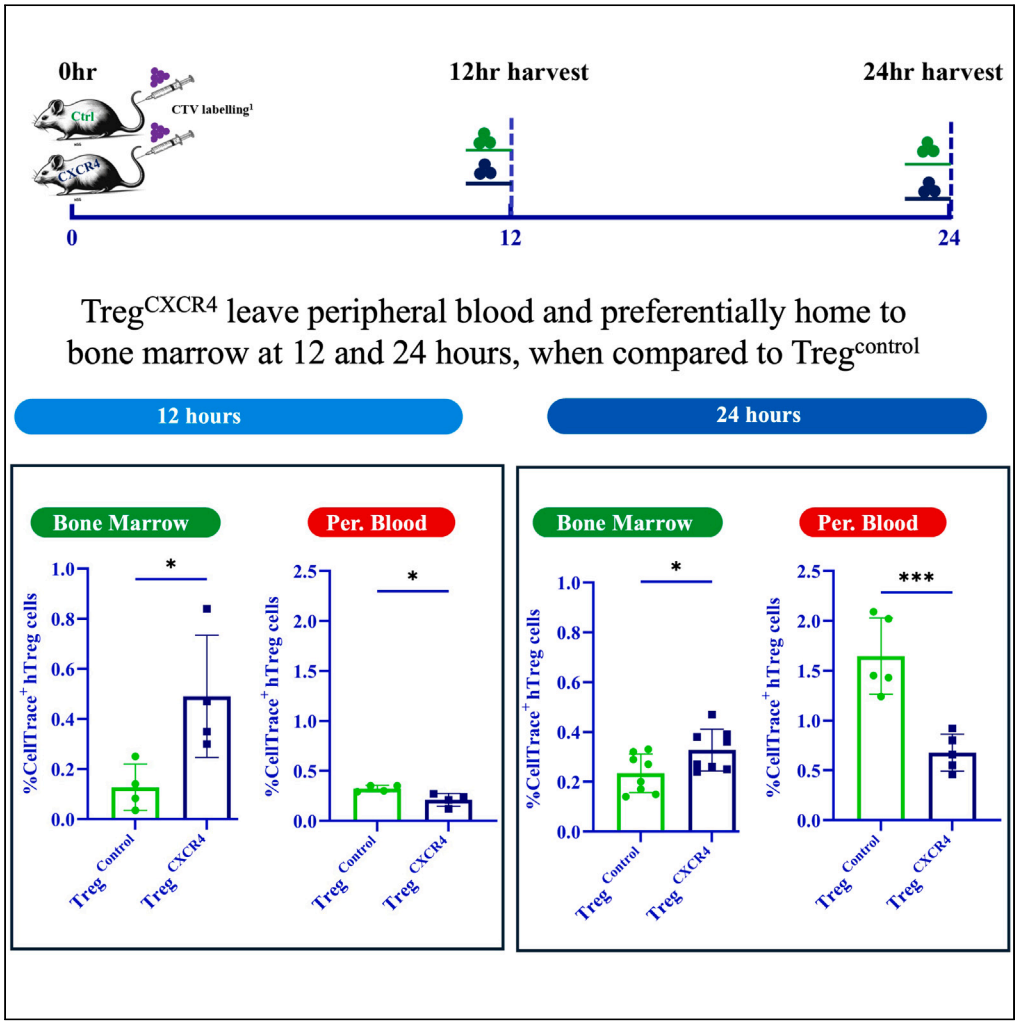


Meixian Huang, Zeng Ke, Mi-Ae Lyu, Lucia Masarova, Tara Sadeghi, Christopher R. Flowers, Simrit Parmar

simrit.parmar@gmail.com

## Highlights

CXCR4-enriched Tregs ($Treg^{CXCR4}$) exhibit upregulation of FoxP3, Helios, and IL-10

$Treg^{CXCR4}$ transit faster toward CXCL12/SDF-1α ligand compared to $Treg^{control}$

$Treg^{CXCR4}$ preferentially home to bone marrow to decrease CD8, IFN-γ, and TNF-α expression

$Treg^{CXCR4}$ decrease TGF-β1/β2 and IFN-γ levels in plasma

Huang et al., iScience 27, 110830
September 20, 2024 
https://doi.org/10.1016/j.isci.2024.110830

iScience

CellPress
OPEN ACCESS

Article

# CXCR4-enriched T regulatory cells preferentially home to bone marrow and resolve inflammation

Meixian Huang,[1] Zeng Ke,[1] Mi-Ae Lyu,[1] Lucia Masarova,[2] Tara Sadeghi,[3] Christopher R. Flowers,[1] and Simrit Parmar[1,4,*]

## SUMMARY

**CXCR4 cell surface expression is critical for the homing of T regulatory (Treg) cells to the bone marrow (BM). We hypothesize that CXCR4 enrichment on Tregs cell surface may abbreviate their transit time to reach BM. Umbilical cord-blood CD25$^+$ Tregs underwent CXCR4 dual enrichment and *ex vivo* expansion using the CRANE process to generate CXCR4-enriched Tregs (Treg$^{CXCR4}$) cells, which showed a faster migration across the Transwell membrane toward CXCL12/stromal cell-derived factor 1α (SDF1α) at 15, 30, and 60 min, when compared to unmanipulated Treg$^{control}$ cells ($p < 0.0001$). Treg$^{CXCR4}$ exhibited preferential homing to BM *in vivo* at 12 and 24 h. Metacluster analysis of BM showed a decrease in CD8$^+$ and an increase in CD39 and CD73 and CXCR5 when compared to Treg$^{control}$. Treg$^{CXCR4}$ decreased plasma TGF-β1/β2 and IFN-γ levels. When compared to control, Treg$^{CXCR4}$ cells decreased in CD8$^+$ T cell, IFN-γ, and TNF-α expression in BM. We conclude that Treg$^{CXCR4}$ show enhanced migration toward CXCL12/SDF1α and a preferential homing to BM resulting in resolution of inflammation.**

## INTRODUCTION

Adoptive therapy with umbilical cord blood (UCB)-derived regulatory T cells (Tregs) can resolve lung inflammation,[1–3] prevent graft vs. host disease,[4–6] treat bone marrow (BM) failure,[7] and improve albuminuria in lupus nephritis.[8] Treg cell migration requires tissue-specific cues involving integrins, chemokine, and other G protein-coupled receptors.[9] Specifically, CXCR4 signaling has been shown to play a critical role in the homing of Tregs to the bone marrow, where blocking CXCR4 decreases human Treg bone marrow trafficking,[10] and ablation of CXCR4 in Treg cells *in vivo* resulted in their moderate but statistically significant decrease in the bone marrow.[11] Therefore, we hypothesize that CXCR4 enrichment would generate a relatively homogenous Treg cell population, which would result in a relatively quantified payload delivery of these cells. Especially in diseases such as myelofibrosis, where the CXCR4/CXCl12 axis plays a major role in the disease pathogenesis,[12] with a larger role for uncontrolled inflammation,[13] CXCR4-enriched Tregs would be an ideal therapeutic candidate.

We also evaluated whether the regulatory/suppressor function of the CXCR4-enriched Treg cells would be different from the control Treg cells based on their differences in the migratory capacity.[14]

## RESULTS

### Dual enrichment of UCB Treg cells leads to higher CXCR4 cell surface expression and faster homing to its ligand SDF1α

Post CD25 enrichment,[1] the cell surface expression of CD4$^+$25$^{hi}$127$^{lo}$ increased from 34.8% to 80.2%, and the co-expression of intracellular FoxP3 and Helios increased from 10.6% to 76.8% when gated on CD4$^+$ T cells, 17.6%–91.9% when gated on CD4$^+$25 $^{hi}$127$^{lo}$ Tregs, and remained unchanged at 6.3%–10.1% when gated on CD4$^+$25$^-$ conventional T cell (Tcon), compared to their respective levels prior to CD25 enrichment (Figure 1A; Table S1). A second CXCR4 enrichment of day 3 or 4 cultured cells led to a significant increase in the CXCR4$^{hi}$ cell population (Figures 1B and 1C) from 73.8% ± 11.4% to 95.1% ± 2.8% (Figure 1D). The enrichment process led to an increase in median fluorescence intensity (MFI) of CXCR4 from 25,945 ± 7,320 to 134,065 ± 11,950 ($n = 3$, $p < 0.001$, mean ± SD). After 14 days of culture, CXCR4-enriched Treg cells (Treg$^{CXCR4}$) and control Treg cells (Treg$^{control}$) showed no differences in CD4$^+$8$^+$ (Figure 1E) or CD4$^+$25 $^+$ 127$^{lo}$ cell populations (Figure 1F). These populations are shown in Figure 1G. The percent of *FOXP3* demethylation in Tcon, Treg$^{control}$, and Treg$^{CXCR4}$ was 3.9 ± 0.8, 52.5 ± 14.4, and 60.4 ± 19.5, respectively (Figure 1H, $p < 0.0001$). Additionally, when compared to Treg$^{CXCR4negative}$, the Treg$^{CXCR4}$ cells showed a higher percent of *FOXP3* demethylation (41.0 ± 25.9 vs. 72.3 ± 10.3, $p = 0.03$, Figure 1I). In order to examine the impact of CXCR4 enrichment on their function, Treg$^{CXCR4}$ and Treg$^{control}$ cells were activated with CD3/CD28 beads and IL-2, revealing no discernible

[1]Department of Lymphoma/ Myeloma, MD Anderson Cancer Center, Houston, TX, USA
[2]Department of Leukemia, MD Anderson Cancer Center, Houston, TX, USA
[3]Cellenkos Inc., Houston, TX, USA
[4]Lead contact
*Correspondence: simrit.parmar@gmail.com
https://doi.org/10.1016/j.isci.2024.110830

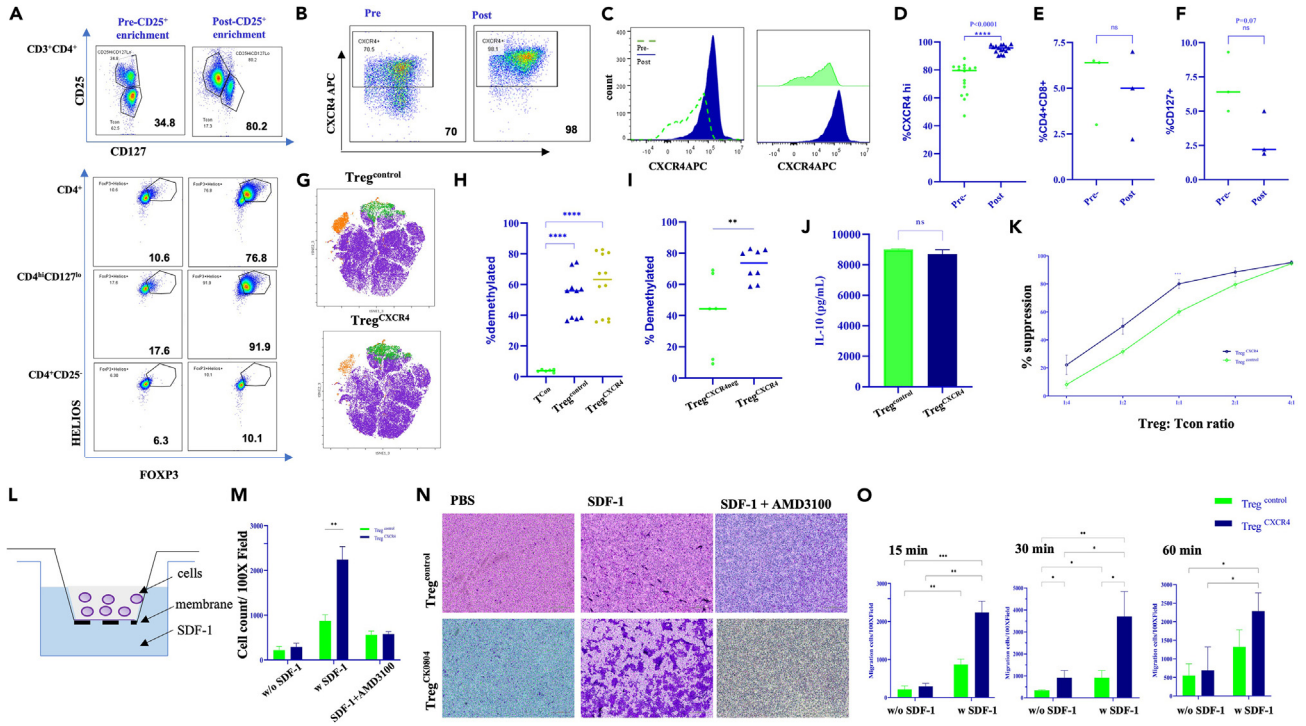


**Figure 1. CXCR4-enriched Tregs home faster to SDF1α**

(A) Fluorescence-activated cell sorting (FACS) plots were utilized to compare the percentages of $CD4^+CD25^{hi}CD127^{lo}$ cells and the co-expression of FoxP3 and Helios in Treg cells before and after CD25 enrichment in day 0 UCB mononuclear cells (MNCs). Upper: the identification of $CD4^+CD25^{hi}CD127^{lo}$ Tregs from $CD3^+CD4^+$ T cells was shown, lower: while the co-expression of FoxP3 and Helios in the indicated $CD4^+$ T cells, $CD4^+CD25^{hi}CD127^{lo}$ Tregs, or $CD3^+CD4^+CD25^-$ Tcon gates was depicted.

(B) Dot plots and (C) histograms illustrating the expression of CXCR4 in day 4 Treg cells before and after CXCR4 enrichment ($Treg^{control}$ and $Treg^{CXCR4}$).

(D) The percentage of $CXCR4^{hi}$ cells among day 3 or day 4 $Treg^{control}$ and $Treg^{CXCR4}$ cells was reported. Data were presented as mean ± standard deviation (SD); $n = 16$; $^{****}p < 0.0001$; unpaired t test.

(E) $CD4^+CD8^+$ co-expression and (F) $CD127^+$ expression ($n = 3$) and (G) t-SNE plot visualization of $CD4^+CD8^+$ (green) and $CD127^+$ (orange) subpopulations overlaid on day 14 expansion pre-and post- CXCR4 Tregs (purple).

(H) The demethylation status of FoxP3, located in intron 1, was significantly higher in expanding $Treg^{control}$ and $Treg^{CXCR4}$ compared to Tcons. Data were presented as mean ± SD; Tcons, $n = 6$ to 12; $^{****}p < 0.0001$; one-way ANOVA.

(I) In comparison to $Treg^{CXCR4neg}$, the FoxP3 gene exhibited higher levels of demethylation in $Treg^{CXCR4}$. Data were analyzed as mean ± SD; $n = 6$ to 8; $^*p < 0.05$; unpaired t test.

(J) $Treg^{control}$ and $Treg^{CXCR4}$ cells were activated with CD3/CD28 beads and IL-2. Following a 24-h incubation, IL-10 levels in the supernatant of the cell cultures were quantified using ELISA. The data were presented as mean ± SD; $n = 2$; $p$ = ns; unpaired t test.

(K) The average percentage of inhibition of Tcon proliferation by $Treg^{control}$ and $Treg^{CXCR4}$ cells at various Treg:Tcon ratios was determined. At a 1:1 ratio, $Treg^{CXCR4}$ cells demonstrated a greater inhibition compared to $Treg^{control}$ cells. $^{***}p < 0.001$; $n = 12$; two-way ANOVA tests; mean ± SD.

(L) Diagrammatic representation of Transwell system.

(M) $Treg^{CXCR4}$ cells show enhanced migration to CXCL12/SDF1α compared to $Treg^{control}$, which is inhibited by CXCR4 antagonist. Upper chamber was plated with $1 \times 10^6$ $Treg^{CXCR4}$ or $Treg^{control}$ cells. Either PBS, CXCL12/SDF1α, or CXCL12/SDF1α+AMD3100 was added to the bottom chamber. At 15 min post plating of the upper chamber, the number of cell migrated to the bottom chamber was counted and recorded ($n = 3$, $p < 0.001$).

(N) Representative images were captured of migrated $Treg^{control}$ and $Treg^{CXCR4}$ cells (purple stained) in response to CXCL12/SDF1α in the presence or absence of AMD3100, on insert membranes at 15 min post plating.

(O) The absolute number of migrated cells on the membranes was quantified. $Treg^{CXCR4}$ cells demonstrated heightened migration toward SDF-1 in comparison to $Treg^{control}$ cells, as evidenced by cell counts of 2,240 ± 241 vs. 871 ± 113 at 15 min, 3,708 ± 924 vs. 922 ± 263 at 30 min, and 2,286 ± 400 vs. 1,325 ± 37 at 60 min. Statistical significance was indicated by $^*p < 0.05$ and $^{**}p < 0.01$; two-way ANOVA test; mean ± SD.

disparities in the secretion of suppressor cytokine, IL-10 (Figure 1J), whereas a significantly higher suppression of Tcon cell proliferation by $Treg^{CXCR4}$ (80.1 ± 11.3%) was observed at a 1:1 ratio when compared to $Treg^{control}$ cells (60% ± 8.4%) ($p < 0.001$, Figure 1K).

CXCL12, also known as stromal cell-derived factor 1 (SDF-1), is a ligand for CXCR4 and a chemoattractant in the bone marrow.[15] Transwell membrane experiment was set as described earlier to examine the egress of $Treg^{CXCR4}$ vs. $Treg^{control}$ across the membrane and toward the chemoattractant, CXCL12/SDF1α (Figure 1L). As shown in Figure 1M, when compared to $Treg^{control}$ cells, as early at 15 min time point, a significantly higher number of $Treg^{CXCR4}$ cells migrated toward CXCL12/SDF1α, across the Transwell membrane into the lower chamber

($n$ = 3, $p$ = 0.0019, Figure S1). This migration effect was predictably blocked by the addition of CXCR4 antagonist, AMD3100.[10] Photomicrograph of representative experiment is shown in Figure 1N. Migration advantage of Treg$^{CXCR4}$ cells over Treg$^{control}$ cells was maintained at 15, 30, and 60 min (Figures 1O and S2).

## Functional and immunophenotypic diversity for Treg$^{control}$ and Treg$^{CXCR4}$ revealed by viSNE visualization

T helper (Th)-like Treg subsets, also referred to as polarized Treg subsets, demonstrate functional diversity, facilitated by their shared homing receptor distribution, which enables effective colocalization. To assess the impact of CXCR4 enrichment on Th-like Treg subsets within Treg$^{control}$ and Treg$^{CXCR4}$ populations, viSNE was utilized for visualization of high-dimensional single-cell data. Figure 2A illustrated that an increase in CXCR4 expression was accompanied by a reduction in chemokine receptors such as CXCR5 (Tf-Treg), CXCR3 (Th1-Treg), CCR4 (Th2-Treg), and CCR6 (Th-17 Treg). In Th17-like Treg cells, a decrease in the MFI of CCR6 expression was noted in Treg$^{CXCR4}$ (492 $\pm$ 142) compared to Treg$^{control}$ (633 $\pm$ 46) cells, along with a decrease in IL-17A secretion (0.9 $\pm$ 0.3 vs. 3.7 $\pm$ 2.3 pg/mL, $n$ = 4) (Figure 2B). Consistent interrelationships among chemokine receptors, transcriptional regulators, and cytokine production were observed. viSNE plots revealed an upregulation of suppression markers FoxP3, Helios, IL-10, and pSTAT5 in Treg$^{CXCR4}$, while a downregulation was observed in T-bet and IFN-γ (Th1-Treg), IL-4 (Th2-Treg), and IL-17 (Th17-Treg) compared to Treg$^{control}$ (Figure 2C). Manual gating on the CD4$^{+}$CD25$^{+}$CD127$^{-}$ Treg cell population confirmed these findings, defining four subsets of Th-like Tregs as Th1-like (CD45RO$^{+}$CXCR3$^{+}$), Th2-like (CD45RO$^{+}$CXCR3$^{-}$CCR6$^{-}$CCR4$^{+}$), Th17-like (CD45RO$^{+}$CXCR3$^{-}$CCR6$^{+}$), and Tf-Tregs (CXCR5$^{+}$). These subsets depicted on the viSNE map were color-coded as follows: CXCR4 Treg in purple, Th1-Treg in yellow, Th2-Treg in orange, Tf-Treg in light blue, and Th17-Treg in green (Figure 2D). The percentages of Th1 and Th2-Tregs (ranging from 4.3% to 6.8%) were found to be decreased in Treg$^{CXCR4}$ compared to Treg$^{control}$, while remaining stable in Th17-Tregs and Tf-Tregs (ranging from 0.3% to 2.6%) (Figure 2E; Tables S2–S4). Therefore, the high CXCR4 expression on Treg$^{CXCR4}$ cells, accompanied by a relative decrease in other homing receptors including CXCR5, CXCR3, CCR4, and CCR6, supports their preferential homing to its ligand CXCL12/SDF-1α expressed in bone marrow and other tissues.

The visualization of viSNE was utilized to assess the immunophenotypic diversity of regulatory mechanisms for Treg$^{control}$ and Treg$^{CXCR4}$. Our findings revealed that Treg$^{CXCR4}$ exhibited elevated expression levels of the Treg-associated marker CD25 and TNF receptor superfamily protein GITR compared to Treg$^{control}$. Conversely, there was a downregulation of the antiapoptotic protein BCL-2 in Treg$^{CXCR4}$ relative to Treg$^{control}$ (Figure 2F). To investigate the homeostasis and functional capabilities of Treg cells, a viSNE plot was employed to visualize the differentiation and activation markers. Our findings highlighted distinct Treg subsets, including central Treg, memory Treg, and effector Treg within Treg$^{control}$ and Treg$^{CXCR4}$. An upregulation of CD62L, CD45RA/RO, CD39, and HLA-DR was observed in Treg$^{CXCR4}$ (Figure 2G). Furthermore, cell clustering revealed a small proportion of functional heterogeneity within Treg cell subsets, characterized by high expression levels of CD39, HLA-DR, and PD-1. Specifically, the CD39$^{hi}$ phenotype in Treg$^{CXCR4}$ displayed a significantly higher CD39 MFI of 38,527 vs. 29,762 in Treg$^{control}$, while the expression of CD73 increased from undetectable levels to an MFI of 4,450 in Treg$^{CXCR4}$, suggesting a potentially enhanced suppressive capacity in this subset. Similarly, HLA-DR$^{hi}$ cell populations increased in Treg$^{CXCR4}$, rising from MFI of 93,302 in Treg$^{control}$ to MFI of 95,152 in Treg$^{CXCR4}$. These characteristics were visualized on a viSNE landscape, where individual cells were color-coded to represent the level of marker expression (Figures 2G and 2H). The gating strategies were clearly outlined, and the accompanying heatmap enabled a thorough evaluation of the phenotypic changes in Treg cells, facilitating a direct comparison of expression profiles between Treg$^{control}$ and Treg$^{CXCR4}$ (Figures 2H and 2I).

## Treg$^{CXCR4}$ preferentially home to bone marrow via the CXCR4/CXCL12 axis *in vivo*

To investigate the *in vivo* migration of Tregs enriched on CXCR4 and determine the potential role of CXCL12 in conferring tissue-specific functional properties to Treg cells, a xenogeneic NSG mouse model was employed. Twelve and 24 h after tail vein injection of CellTrace Violet (CTV)-labeled Treg$^{CXCR4}$ or Treg$^{control}$ cells, mice were euthanized and different tissues including BM, peripheral blood (PB), liver, and spleen were analyzed (Figure 3A). At the 12- and 24-h (Figure 3B) interval, Treg$^{CXCR4}$ cells exhibited a significantly superior homing to BM compared to Treg$^{control}$ (Figure 3C; $p$ = 0.0319, $n$ = 4 and $p$ = 0.0362, $n$ = 5). While an increase in CTV-labeled Treg$^{CXCR4}$ cells was observed in the spleen ($p$ = 0.0356) and liver ($p$ = 0.0304), such difference was not detected at 24 h in the spleen ($p$ = 0.9) and was, in fact, reversed in the liver ($p$ = 0.008). In stark contrast, Treg$^{CXCR4}$ cells were significantly less prevalent in PB at 12 ($p$ = 0.0009) and 24 h ($p$ = 0.0079) compared to Treg$^{control}$. In BM, the Treg homing index,[16] calculated as a measure of the relative abundance of Treg$^{CXCR4}$ to Treg$^{control}$, rose significantly from their initial measurement to 12 h ($p$ = 0.0006), a trend that, while attenuated, remained significant at 24 h ($p$ = 0.0263) (Figure 3D), with a corresponding decline in PB at the same time points ($p$ = 0.0186 and $p$ = 0.0028, respectively). While the Treg homing index for Treg$^{CXCR4}$ when compared to Treg$^{control}$ increased markedly at 12 h in the spleen ($p$ = 0.0003), it returned to its initial levels by 24 h ($p$ = ns). The findings on the migration of Treg$^{CXCR4}$ cells may play a role in shaping their tissue-specific functional characteristics, with a focus on their tendency to migrate preferentially to CXCL12-rich environments in the bone marrow and spleen, facilitated by the CXCL12-CXCR4 axis (Figures 1L–1O).

To further elucidate the involvement of the CXCL12-CXCR4 axis in Treg cell homing, we conducted a comparative analysis of CXCR4 expression levels on human Treg$^{control}$ cells and Treg$^{CXCR4}$ cells, as well as the human and murine cross-reactive CXCL12 on murine bone marrow and spleen stromal cells following Treg infusion at 24 h. Consistent patterns in the levels of the CXCL12-CXCR4 axis and the homing index were observed in both BM and spleen (Figure 3D). Our study revealed a significantly higher expression of MFI CXCR4 on human Treg$^{CXCR4}$ cells (11.5 × 10$^{4}$) compared to Treg$^{control}$ cells (9.4 × 10$^{4}$) in the bone marrow (Figure 3E). Notably, there was a significant increase in the Treg$^{CXCR4}$ group in terms of cross-reactive CXCL12 expression on murine BM stromal cells compared to Treg$^{control}$ group ($p$ = 0.011), while no significant changes were noted in the murine spleen ($p$ = ns) (Figure 3F).

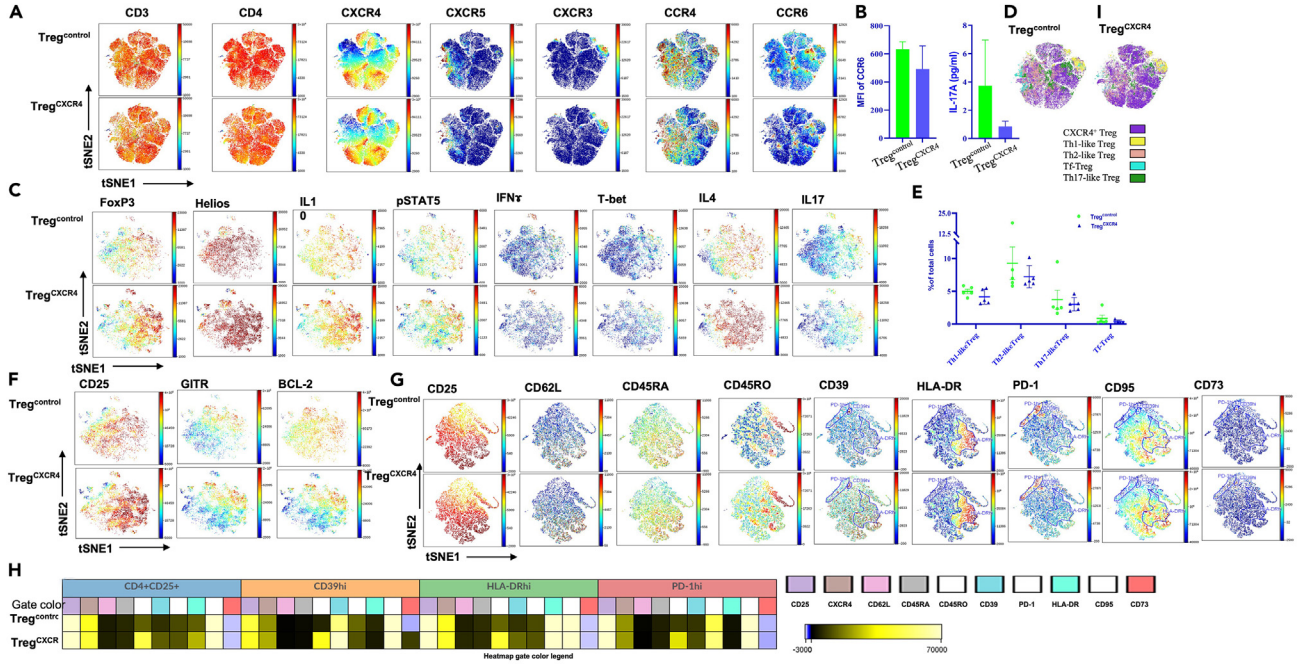


**Figure 2. Functional and immunophenotypic diversity for Treg$^{control}$ and Treg$^{CXCR4}$ revealed by viSNE visualization**

(A) viSNE visualization was used to illustrate the varying expression intensity of chemokine receptors (CXCR5, CXCR3, CCR6, and CCR4) among different Treg subtypes (Tf-Treg, Th1-like Treg, Th17-like Treg, and Th2-like Tregs) in Treg$^{control}$ and Treg$^{CXCR4}$, revealing the identification of distinct immunophenotypic classifications.

(B) Comparative analysis of CCR6 expression and IL-17 levels between Treg$^{control}$ and Treg$^{CXCR4}$ revealed that Treg$^{CXCR4}$ displayed lower CCR6 expression and reduced IL-17 levels in the cell culture supernatant (mean ± SD; $n = 4$; unpaired t test).

(C) viSNE plots characterizing representative transcriptional regulators for Treg$^{control}$ and Treg$^{CXCR4}$ with upregulation of FoxP3, Helios, IL-10, and pSTAT5 in Treg$^{CXCR4}$ and a downregulation of T-bet and IFN-γ (Th1-like Treg subset), IL-4 (Th2-like Treg), and IL-17 (Th17-like Treg) compared to Treg$^{control}$.

(D) The subsets on the viSNE map were color-coded as follows: CXCR4$^{Treg}$ in purple, Th1-like Treg in yellow, Th2-like Treg in orange, Tf-Treg in light blue, and Th17-like Treg in green ($n = 4$; Tables S2–S4).

(E) Comparison of percentages of Th-like Tregs between Treg$^{control}$ and Treg$^{CXCR4}$ revealed that Th-like Tregs and Tf-Treg subsets decreased in Treg$^{CXCR4}$ compared to Treg$^{control}$ ($n = 5$, mean ± SD, Tables S2–S4).

(F) viSNE map visualization illustrating the varying expression levels of Treg-associated marker CD25, the TNF receptor superfamily protein GITR, antiapoptotic protein BCL-2. Each marker was depicted with a unique color gradient, depicting their distribution in Treg$^{control}$ and Treg$^{CXCR4}$.

(G) viSNE plot effectively demonstrated the differentiation of Treg$^{control}$ and Treg$^{CXCR4}$, emphasizing specific markers associated with CD62L$^{hi}$CD45RA$^{hi}$ central Treg (cTreg), CD45RA$^{lo}$CD45RO$^{hi}$ memory Treg (mTreg), CD45RA$^{lo}$CD45RO$^{hi}$HLA-DR$^{hi}$ effector Treg (eTreg) cells. Additionally, distinct cell clustering was observed among adenosine signaling markers (CD39 and CD73), inhibitory receptor PD-1, and effector markers (HLA-DR and CD95), leading to the identification of a small proportion of heterogeneous Treg subsets characterized by the expression level of CD39$^{hi}$, PD-1$^{hi}$, and HLA-DR$^{hi}$.

(H) These findings were further supported by heatmap analysis.

(I) The heatmap showed expression patterns on the viSNE landscape with clear gating strategies, assigning colors based on marker intensity for detailed analysis of phenotypic complexity and comparison between Treg$^{control}$ and Treg$^{CXCR4}$.

Our recent clinical trial[17] results demonstrate an increase in FOXP3$^{+}$CD4$^{+}$ T cells in the bone marrow biopsy of a patient with aplastic anemia after treatment with CK0801 (Treg$^{control}$) on day +30, indicating a potential correlation with improved transfusion requirements.[7] Additionally, a viSNE plot was utilized to visualize the localization of human Treg$^{control}$ and Treg$^{CXCR4}$ cells in the bone marrow of NSG murine recipients, distinguishing murine hematopoietic (mCD45$^{+}$) and BM stromal and endothelial cells (CD45$^{-}$CXCL12$^{+}$). The increased expression of CXCL12 in murine bone marrow stromal and endosteal regions, particularly in the Treg$^{CXCR4}$ group, was associated with higher levels of CXCR4-positive expression in human Treg$^{CXCR4}$ compared to Treg$^{control}$ (Figure 3G). This homing pattern suggested that Treg$^{CXCR4}$ preferentially home to the bone marrow via the CXCR4/CXCL12 axis *in vivo*, potentially resolving inflammation in the bone marrow.

## Immune assessment of bone marrow Tregs

Bone marrow samples were analyzed using t-SNE to visualize metaclusters 6, 7, and 10, which exhibited a higher presence in Treg$^{CXCR4}$ recipients compared to Treg$^{control}$ recipients ($n = 3$ $p = 0.044$, *$p = 0.016$, and $p = 0.663$, respectively, as shown in Figures 4A, 4B, and 4C). The distribution of cell populations between Treg$^{CXCR4}$ and Treg$^{control}$ recipients within these metaclusters revealed an overall increase in CD4$^{+}$, a decrease in CD8$^{+}$, and an increase in the expression of CD39, CD73, and CXCR5. While an increase in CCR6 expression was noted in

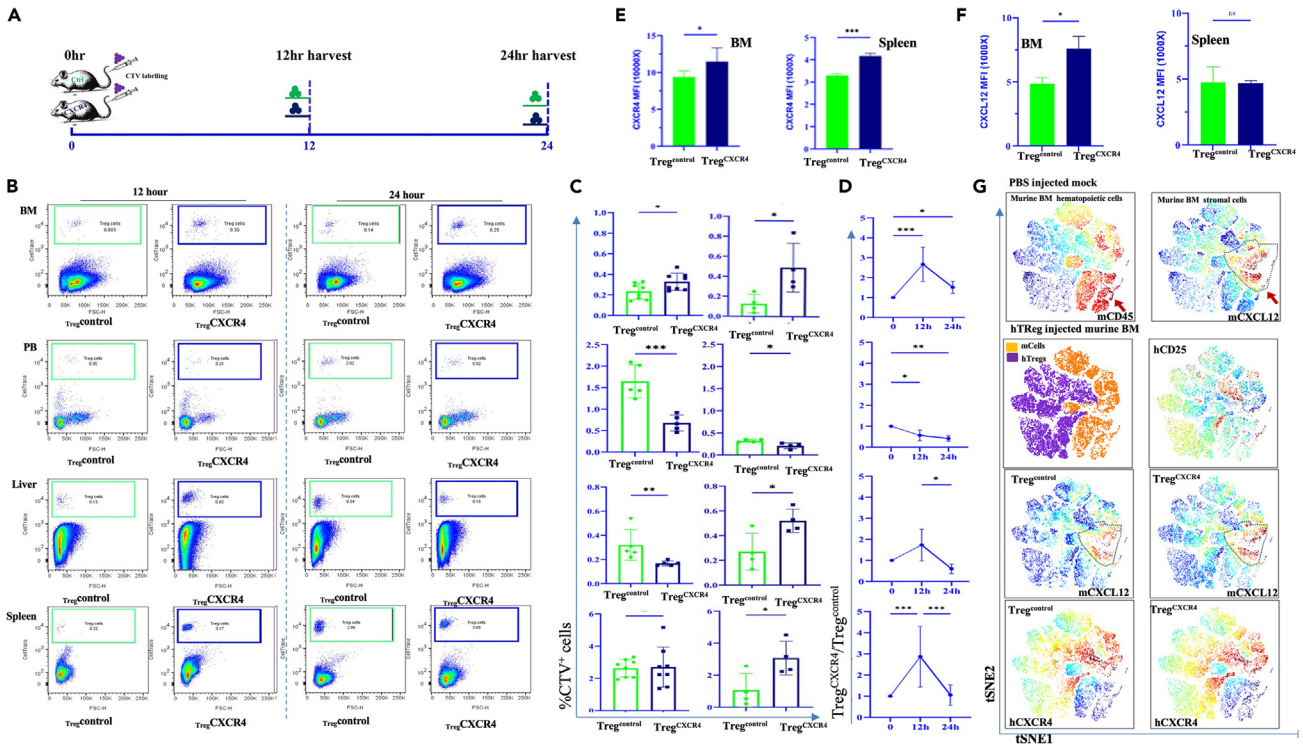


**Figure 3. CXCR4 determines preferential homing of Treg$^{CXCR4}$ cells to the BM and spleen when compared to Treg$^{control}$ cells**

(A) *In vivo* homing experimental design schematic. NSG mice were injected through tail vein with 1 × $10^7$ Treg$^{CXCR4}$ or Treg$^{Control}$ cells and were euthanized at 12 and 24 h to harvest organs including bone marrow (BM), spleen (SP), liver (LV), and peripheral blood (PB).

(B) Representative plots of CellTrace Violet (CTV)-labeled human Treg$^{CXCR4}$ (right column, blue gating) versus Treg$^{Control}$ cells (left column, green gating) in the BM, PB, LV, and SP at 12 and 24 h post injection.

(C) Quantitative analysis of Treg$^{CXCR4}$ versus Treg$^{Control}$ cells at 12 ($n$ = 4) and 24 h ($n$ = 5) in BM, PB, liver, and spleen; $p$ = 0.03, 0.02, 0.03, and 0.03, respectively for 12 h, and $p$ = 0.03, 0.0009, 0.008, and 0.9, respectively.

(D) Homing index calculated as ratio of Treg$^{CXCR4}$ to Treg$^{Control}$ in BM, PB, liver, and spleen at 12 (left column) and 24 h (right column) post-cell infusion. The homing index was derived from the ratio of Treg$^{CXCR4}$ to Treg$^{Control}$ cells within each organ. Percentages denoted the proportion of cells that have migrated to each tissue at the specified time intervals. Data were presented as mean ± SD for a sample size of $n$ = 4 mice per group at 12 h, and $n$ = 8 for BM and spleen, $n$ = 5 for PB and liver at 24 h. Statistical evaluations were performed using unpaired t tests and one-way ANOVA to determine significance levels (*$p$ < 0.05; **$p$ < 0.01; ***$p$ < 0.001).

(E) Quantitative analysis of CXCR4 mean fluorescence intensity (MFI) on human Treg$^{CXCR4}$ and Treg$^{Control}$ cells derived from murine bone marrow and spleen.

(F) The levels of human and murine cross-reactive CXCL12 expression in stromal cells from murine bone marrow and spleen were compared between Treg$^{Control}$ and Treg$^{CXCR4}$ groups at 24 h. Values for (E) and (F), presented as mean ± SD for $n$ = 3, Student's t test, *$p$ < 0.05 ***$p$ < 0.001, and ****$p$ < 0.0001.

(G) viSNE plotted 12,500 cells from mock-PBS and Treg-infusion murine BM (top), distinguishing hematopoietic and stromal and endothelial cells (middle to bottom). Top: differentiated between hematopoietic cells and stromal cells in the bone marrow using a color gradient based on mouse CD45 and cross-reactive CXCL12. Cells were colored by cell type and expression of CD25 (upper middle). The viSNE map also displayed the expression of cross-reactive CXCL12 in murine BM stromal cells (lower middle) and the level of human CXCR4 expression (bottom panel) in the Treg$^{Control}$ (left) and Treg$^{CXCR4}$ groups (right).

metacluster 6 and a decrease in metacluster 7, these differences were not significant. Additionally, the distribution of CD45RA across the three metaclusters did not show statistically significant differences. In metacluster 7, there was an observed increase in co-expression for CD39, CD73, and CXCR5, while a decrease was noted for CD45RA, CD95, HLA-DR, CD8, and CD127 in Treg$^{CXCR4}$ compared to Treg$^{control}$ recipients (Figures 4D and 4E). This finding was further supported by the heatmap illustrating their expression profile (Figure 4F). Additionally, human Treg$^{CXCR4}$ cells in murine BM recipients showed a stronger correlation with CD39 and a weaker correlation with CD95, HLA-DR, and CCR6 within the metacluster 7, as compared to Treg$^{control}$ recipients (Figure 4G).

## Treg$^{CXCR4}$ decrease TGF-β and other plasma cytokines

The plasma levels of TGF-β1 and TGF-β2 were found to be significantly reduced at 24 h in Treg$^{CXCR4}$ recipients compared to Treg$^{control}$ recipients (Figure 5A). Additionally, a heatmap depicting the levels of various plasma cytokines including EGF, Eotaxin, FGF2, FLT-3L, IFN-α2, IL-13, IL-17E/IL-25, IL-27, IP-10, MCP-1, MCP-3, MIP-1β, PDGF AB/BB, and TGF-α at 24 h post-Treg cell injection showed a reduction in their levels among Treg$^{CXCR4}$ recipients compared to Treg$^{control}$ recipients (Figure 5B). Both the Treg$^{CXCR4}$ and Treg$^{control}$ groups showed low levels

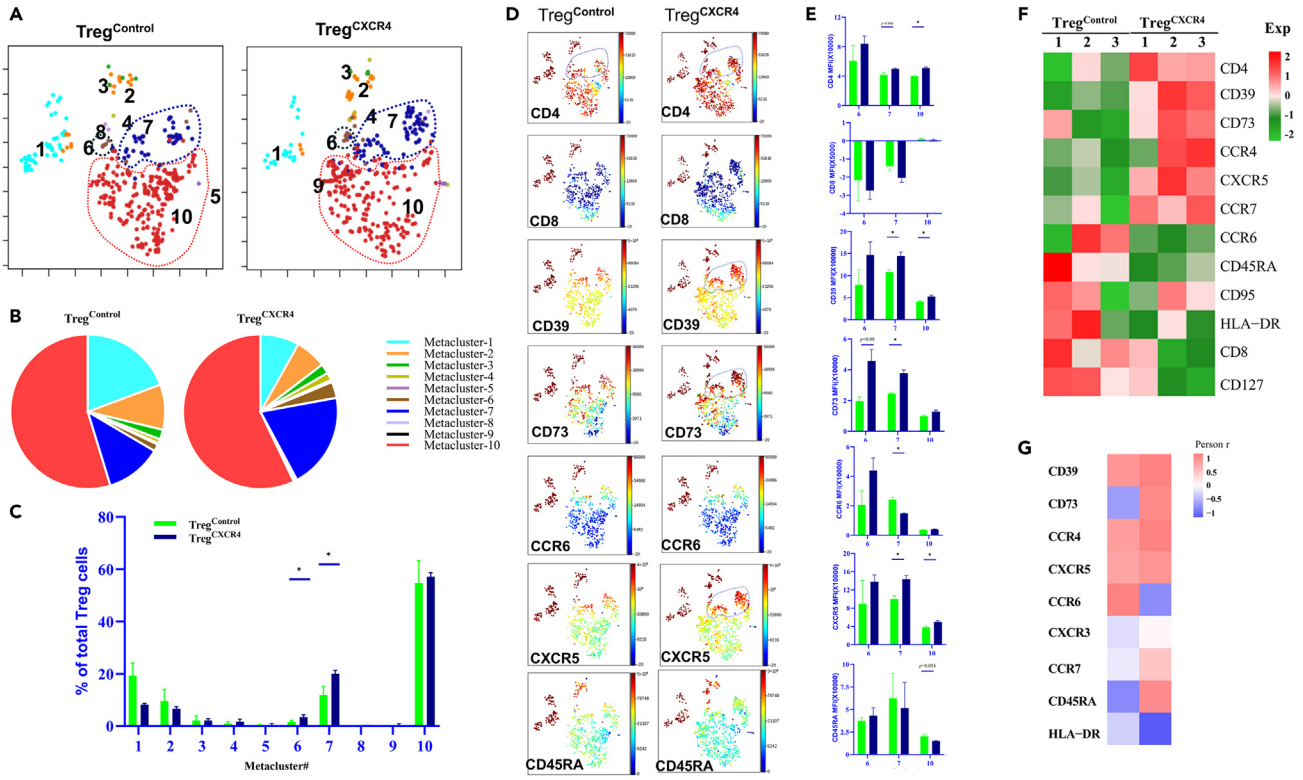


**Figure 4. Immune assessment of BM Tregs**

t-SNE plot of FlowSOM metaclusters analysis of human Treg$^{control}$ and Treg$^{CXCR4}$ samples in mouse bone marrow BM recipients.

(A) Each metacluster identified by a unique color and (B) representative percentage was shown in the pie charts of Treg$^{control}$ (left) and Treg$^{CXCR4}$ (right).

(C) Bar graph showing frequency of each metacluster derived from murine bone marrow of human Treg$^{control}$ and Treg$^{CXCR4}$ cells recipients. Metacluster 6, 7, and 10 had a higher presence of Treg$^{CXCR4}$ compared to Treg$^{control}$ (mean ± SD, for $n = 3$, Student's t test, *$p = 0.044$, *$p = 0.016$, and $p = 0.663$).

(D) Higher expression of CD4, CD39, CD73, and CXCR5 was observed, particularly in metacluster 7.

(E) Quantitative levels of CD4, CD8, CD39, CD73, CCR6, CXCR5, and CD45RA in the Treg$^{CXCR4}$ compared to Treg$^{control}$ within metacluster 7 are presented as mean ± SD for $n = 3$, Student's t test, *$p < 0.05$.

(F) Heatmap of FlowSOM metacluster 7 revealed higher expression of suppression markers CD39 and CD73, as well as homing markers CCR4, CXCR5, and CCR7 in Treg$^{CXCR4}$ compared to Treg$^{control}$. Additionally, Treg$^{CXCR4}$ exhibit lower expression of CD45RA, CD95, HLA-DR, CD8, and CD127.

(G) Mouse bone marrow samples from recipients human Treg$^{CXCR4}$ or Treg$^{control}$ demonstrated an increased correlation of Treg$^{CXCR4}$ administration with the expression of CD39, CD73, CCR4, CXCR5, CCR7, and CD45RA, while a lower correlation was noted with CCR6 and HLA-DR in metacluster 7. The heatmap of FlowSOM metacluster 7 included Spearman's r coefficients.

of other cytokines such as GROα, IL-4, IL-6, IL-8, IL-9, IL-15, IL-17A, IL-18, M-CSF, MDC, MIG/CXCL9, PDGF-AA, RANTES, TNF-β, and VEGF-A (Table S5).

## Treg$^{CXCR4}$ decrease bone marrow inflammation

To better understand the impact of Treg$^{CXCR4}$ on bone marrow inflammation, immunostaining was performed on bone marrow biopsies from control (peripheral blood mononuclear cell [PBMC] only) and treatment arm (PBMC+Treg$^{CXCR4}$), where two longitudinal samples ($n = 2$, each group) were analyzed. Pseudocolor micrographs were utilized to identify nuclei using DAPI (Figure 5C, upper panel), CD8$^+$ T cells (second row panel), secreted TNF-α (third row panel), and merged images (bottom panel) (Figure 5D). Pseudocolor micrographs were also used to identify IFN-γ (yellow) (Figure 5E) in the treatment group (PBMCs+Treg$^{CXCR4}$) compared to the control group (PBMC only). The corresponding plasma levels of human IFN-γ were significantly decreased in the treatment group (PBMCs+Treg$^{CXCR4}$) compared to the control group (PBMC only) (Figure 5F, Student's t test, ****$p < 0.0001$). Additionally, quantification of the immunofluorescence staining of bone marrow also demonstrated a significant reduction in the levels of TNF-α (Figure 5G, $p = 0.032$) and IFN-γ (Figure 5H, $p = 0.033$), respectively.

## DISCUSSION

Here, we show that enrichment of Tregs on CXCR4 generates a unique cell population with differential cell surface and intracellular profile as well as a higher expression of suppressor markers. Specifically, our data show that CXCR4 enrichment allows for enhanced transit of Treg$^{CXCR4}$

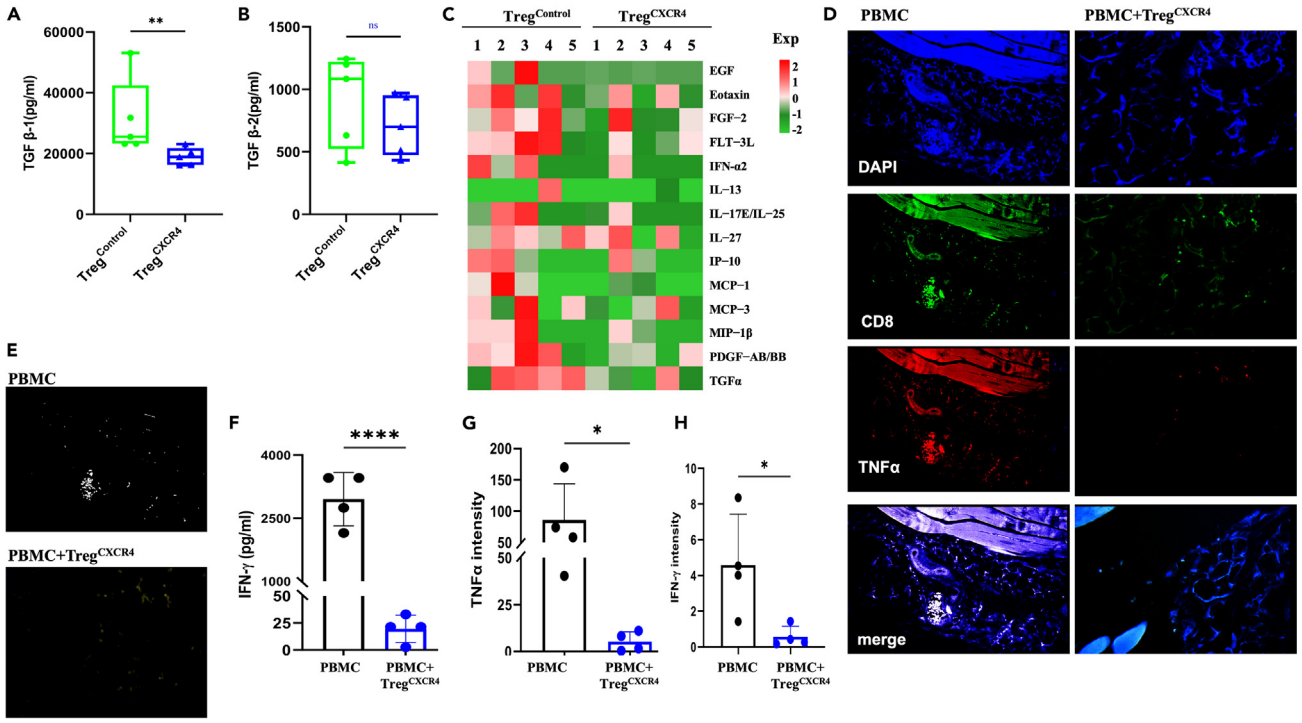


**Figure 5. Treg$^{CXCR4}$ decrease TGF-β1/β2 and bone marrow inflammation**

Mouse plasma was examined for circulating human inflammatory cytokines. Treg$^{CXCR4}$ decreases (A) TGF-β1 and (B) TGF-β2 *in vivo*. Histogram represents the levels of TGF-β1 and TGF-β2 between Treg$^{Control}$ and Treg$^{CXCR4}$ (**$p < 0.01$, t test, $n = 5$ each group).

(C) Comparative analysis of heatmap of cytokine normalized expression profile between Treg$^{Control}$ and Treg$^{CXCR4}$. The color scale ranges from green (low expression) to red (high expression), indicating the relative abundance of each cytokine. A shift toward the green end of the spectrum denotes decreased expression levels of inflammatory cytokines in the Treg$^{CXCR4}$ group. The y axis categorizes the cytokines, while the X axis separates Treg$^{Control}$ and Treg$^{CXCR4}$ ($n = 5$ mice per group; *in vivo* homing assay at 24 h post-injection).

(D) Treg$^{CXCR4}$ decrease bone marrow inflammation. Bone marrow biopsy samples from control (PBMC only) and treatment (PBMC+Treg$^{CXCR4}$) were stained using anti-CD8, anti-TNF-α, and anti-IFN-γ antibodies and imaged using a Leica DMi8 inverted microscope. Representative pseudocolor micrograph of bone marrow: control group (left) and treatment group (right). Blue = DAPI (4′,6-diamidino-2-phenylindole) (upper), green = CD8 (second row), red = TNF-α.

(E) Treg$^{CXCR4}$ decrease IFN-γ in bone marrow. Representative pseudocolor micrograph showing IFN-γ secretion (yellow) by human PBMCs and human PBMCs treated with Treg$^{CXCR4}$ in bone marrow from the Treg$^{CXCR4}$ treatment group (PBMCs+Treg$^{CXCR4}$, right graph).

(F) Treg$^{CXCR4}$ decrease IFN-γ secretion. Plasma levels of human IFN-γ were compared between control and treatment arms. Data indicate mean ± SD of two technical replicates for $n = 2$, Student's t test, ****$p < 0.0001$. Representative intensity of (G) TNF-α and (H) IFN-γ of bone marrow from PBMCs+Treg$^{CXCR4}$ mice ($n = 4$) was found to be significantly lower compared to PBMCs mice ($n = 4$) as determined through immunofluorescence staining and quantification using ImageJ software. Values are presented as mean ± SD of two technical replicates for $n = 2$, Student's t test ($p = 0.0327$ and $p = 0.0333$, *$p < 0.05$).

cells toward chemokine SDF1α *in vitro* as well as to bone marrow *in vivo*. Such a preferential homing to BM was associated with a decrease in plasma TGF-β and IFN-γ levels as well as BM CD8$^+$ T cells, IFN-γ, and TNF-α when compared to unmanipulated Tregs.

Preservation of the low expression of PD-1 in both Treg$^{CXCR4}$ and Treg$^{control}$ cells as observed in our data has important implications, since PD-1 negatively regulates the activation and suppressor function of Tregs, where PD-1-deficient Tregs exhibit an activated phenotype and enhanced immunosuppressive function and are potentially associated with better control of autoimmune diseases.[18] Furthermore, PD-1-deficient Tregs, revealed down-regulation of genes in the PI3K-AKT-mTOR signaling pathway, in gene set enrichment analyses.[19] In fact, even in healthy individuals, high PD-1 expression on human Tregs identifies a dysfunctional, exhausted subset that secretes IFN-γ.[20] Additionally, Treg$^{CXCR4}$ cells retained their co-expression of CD45RA/RO, which is unique to the UCB Tregs, and potentially confer gain of effector function (CD45RO), while retaining their ability to proliferate and maintain their naivity (CD45RA).[1,8]

In the bone marrow, constitutive CXCL12 secretion by stromal cells is crucial for homing and sustaining CXCR4-expressing hematopoietic stem and progenitor cells in their niches.[21,22] Our observation of a reciprocal increase in the CXCL12 expression in the mouse bone marrow stromal cells might be explained by mutual reciprocal interactions between CXCR4 and CXCL12.[23] The bone marrow endothelial and other stromal cell types highly express both CXCR4 receptor and its ligand CXCL12, implying an autocrine loop mechanism to regulate CXCR4 expression on these cells.[24] Acquiring tissue-specific migration as a function of CXCR4 enrichment allowed for increased expression of CD62L, which in turn enabled the homing of Tregs to secondary lymphoid organs.[9]

CXCR4 enrichment also led to an increase in the co-expression of CD39/CD73 that mediates non-antigen-specific suppressive mechanisms of Tregs by leveraging increased adenosine concentration in the microenvironment to inhibit dendritic cell presentation of antigens and suppression of activated T effectors.[25,26] Increased HLA-DR expression in Treg$^{CXCR4}$ support early contact suppressive activity and are essential for Treg suppressor function.[27] Clustered increase in the STAT5 and CD73 expression is also suggestive of the spatiotemporal distribution of the Treg$^{CXCR4}$ to be situated closer to the antigen-presenting cell.[28] It is also possible that change in the migratory profile of Tregs as a result of CXCR4 enrichment might have also led to differences in T cell receptor specificity and affinity as well as allowed for the expression of additional genes responsible for tissue-specific functioning.[26] *In vivo*, Treg$^{CXCR4}$ maintained the high CD39/73 co-expression but had a relative decrease in HLA-DR along with CD95, which might have been a result of co-localization.[29]

Decrease in Th17-like (CD45RO$^{+}$CXCR3$^{-}$CCR6$^{+}$) Tregs that secrete inflammatory cytokines including IL-17 and IL-22 and a corresponding decrease in CCR6, on Tregs cell surface[30,31] accompanied by a decrease in IL-17 secretion, suggest that CXCR4 enrichment selects for a CCR6-deficient Treg cell population that may exhibit differential suppressor function.[32] Additionally, a decrease in Th1-like Treg subset with a corresponding decrease in CXCR3 expression, T-bet[33] and IFN-γ secretion, as well as a decrease in Th2-like Tregs with a corresponding decrease in CCR4 expression and IL-4 secretion, in Treg$^{CXCR4}$ cells, is suggestive of decreased plasticity.[34] CXCR4 enrichment was also associated with increased expression of the bona fide Treg markers including FoxP3 and Helios,[35] IL-10,[36] and pSTAT5,[37] which might explain the differential impact on the inflammatory cytokines *in vivo*.

TGF-β, shown to play a pathogenic role in myelofibrosis,[38] was decreased to a greater extent by Treg$^{CXCR4}$ cells. The ability of Treg$^{CXCR4}$ to preferentially decrease PDGF AB/BB, where PDGF signaling has been identified to play an important role in pathogenesis of myelofibrosis,[39,40] is suggestive of their specific engagement with the culprit pathways engaged in BM inflammation. Additional inflammatory cytokines that are implicated in BM inflammation and fibrosis were also decreased in Treg$^{CXCR4}$ recipients and included (1) EGF and Eotaxin,[41] (2) TGF-α, a polypeptide growth factor structurally and functionally related to EGF,[42] (3) FGF2, associated with BM fibrosis as well as its correlation with TGF-β in myeloproliferative neoplasm (MPN),[43] (4) FLT-3L, which plays an important role in dysmegakaryopoiesis in myelofibrosis,[44] (5) IFN-α2 in BM inflammation,[45] (6) IL-1RA, pathogenic role in MPN disease progression,[46] (7) IL-17E/IL25 in generating reactive oxygen species in BM,[47] (8) IP-10[48] and MIP1β in mediating TH1 type signaling,[49] and (9) MCP-1 and -2, potent chemo-attractant for pathogenic monocytes.[50]

Myelosuppressive cytokines including TNF-α and IFN-γ have been implicated in driving bone marrow inflammation leading to the death of hematopoietic progenitor cells.[51] Additionally, CD8$^{+}$ T cells drive autoimmune hematopoietic stem cell dysfunction.[52] The ability of Treg$^{CXCR4}$ cells to significantly decrease all these three factors compared to the control in a bone marrow inflammation model supports our hypothesis that CXCR4 enrichment of Tregs cells is a viable therapeutic strategy.

In conclusion, we have developed a unique Treg$^{CXCR4}$ cell population that preferentially expresses CD39/73 pathway, is associated with enhanced suppressor function, and homes specifically to the bone marrow to decrease inflammation.

### Limitations of the study

Our study has a few limitations including the xenogeneic bone marrow inflammation model, which might not capture all the elements of the inflammatory processes as well as extramedullary hematopoiesis manifested by complex diseases such as myelofibrosis. Due to limited sampling, an extensive examination of the bone marrow immunophenotype and inflammatory cytokine composition was not performed.

## RESOURCE AVAILABILITY

### Lead contact

Further information and requests for resources should be directed to and will be fulfilled by the corresponding author, Simrit Parmar.

### Materials availability

Treg$^{CXCR4}$ can be accessed through material transfer agreement.

### Data and code availability

- Any additional information required to reanalyze the data reported in this paper is available from the lead contact upon request.
- This paper does not report original code.

## ACKNOWLEDGMENTS

The authors thank Dr. Robert Negrin, Stanford University, for careful review of our manuscript.

## AUTHOR CONTRIBUTIONS

M.H. was responsible for conceptualization, data curation, formal analysis, investigation, methodology, project administration, resources, software, supervision, validation, visualization, writing – original draft, and writing – review and editing. Z.K., M.-A.L., and L.M. were responsible for data curation, formal analysis, investigation, and writing – review and editing. T.S. was responsible for resources, materials, formal analysis, and writing – review and editing. C.R.F. was responsible for funding acquisition, project administration, resources, supervision, validation, and writing – review and editing. S.P. was responsible conceptualization, data curation, formal analysis, funding acquisition, investigation, methodology, project administration, resources, software, supervision, validation, visualization, writing – original draft, and writing – review and editing.

## DECLARATION OF INTERESTS

S.P. has an equity interest in, holds patents for, receives royalties and research funding from, and is a member of the board of directors/advisory committee for Cellenkos Inc. C.R.F. received research funding from 4D, AbbVie, Acerta, Adaptimmune, Allogene, Amgen, Bayer, Celgene, Cellectis, Cellenkos, EMD, Gilead, Genentech/Roche, Guardant, Iovance, Janssen Pharmaceutical, Kite, MorphoSys, Nektar, Novartis, Pfizer, Pharmacyclics, Sanofi, Takeda, TG Therapeutics, Xencor, Ziopharm, Burroughs Wellcome Fund, Eastern Cooperative Oncology Group, National Cancer Institute, and Cancer Prevention and Research Institute of Texas: CPRIT Scholar in Cancer Research and consulting fees from AbbVie, Bayer, BeiGene, CelgeneDenovo Biopharma, Epizyme, Genentech/Roche, Genmab, Gilead, Karyopharm, Pharmacyclics/Janssen, Seagen, and Spectrum. T.S. is an employee of Cellenkos Inc. L.M. is a consultant/advisor/speaker: Cogent, GlaxoSmithKline, MorphoSys, and PharmaEssentia. The authors declare that this study received funding from Cellenkos Inc.

## STAR★METHODS

Detailed methods are provided in the online version of this paper and include the following:

- KEY RESOURCES TABLE
- EXPERIMENTAL MODEL AND STUDY PARTICIPANT DETAILS
  - *In vivo* xenogeneic homing mouse model
  - Bone marrow inflammation xenograft model
  - Institutional approval for animal studies
- METHOD DETAILS
  - UCB Treg cells, and Treg$^{CXCR4}$ cells isolation and *in vitro* expansion
  - Flow cytometry
  - viSNE analysis
  - DNA methylation analysis
  - IL-10 secretion assay
  - Cell suppression assay
  - Migration assay
  - *In* vivo phenotype analysis by flow cytometry
  - Cytokine analysis
  - Bone marrow immunostaining
  - Interferon-γ ELISA
- QUANTIFICATION AND STATISTICAL ANALYSIS

## SUPPLEMENTAL INFORMATION

Supplemental information can be found online at https://doi.org/10.1016/j.isci.2024.110830.

Received: April 12, 2024
Revised: June 15, 2024
Accepted: August 23, 2024
Published: August 27, 2024

## REFERENCES

1. Lyu, M.A., Huang, M., Zeng, K., Li, L., Khoury, J.D., Nishimoto, M., Ma, H., Sadeghi, T., Mukherjee, S., Slutsky, A.S., et al. (2023). Allogeneic cord blood regulatory T cells can resolve lung inflammation. Cytotherapy *25*, 245–253. https://doi.org/10.1016/j.jcyt.2022.10.009.
2. Gladstone, D.E., D'Alessio, F., Howard, C., Lyu, M.A., Mock, J.R., Gibbs, K.W., Abrams, D., Huang, M., Zeng, K., Herlihy, J.P., et al. (2023). Randomized, double-blinded, placebo-controlled trial of allogeneic cord blood T-regulatory cells for treatment of COVID-19 ARDS. Blood Adv. *7*, 3075–3079. https://doi.org/10.1182/bloodadvances.2022009619.
3. Gladstone, D.E., Kim, B.S., Mooney, K., Karaba, A.H., and D'Alessio, F.R. (2020). Regulatory T Cells for Treating Patients With COVID-19 and Acute Respiratory Distress Syndrome: Two Case Reports. Ann. Intern. Med. *173*, 852–853. https://doi.org/10.7326/L20-0681.
4. Kellner, J.N., Delemarre, E.M., Yvon, E., Nierkens, S., Boelens, J.J., McNiece, I., Olson, A., Nieto, Y., Ciurea, S., Popat, U., et al. (2018). Third party, umbilical cord blood derived regulatory T-cells for prevention of graft versus host disease in allogeneic hematopoietic stem cell transplantation: feasibility, safety and immune reconstitution. Oncotarget *9*, 35611–35622. https://doi.org/10.18632/oncotarget.26242.
5. Brunstein, C.G., Miller, J.S., Cao, Q., McKenna, D.H., Hippen, K.L., Curtsinger, J., Defor, T., Levine, B.L., June, C.H., Rubinstein, P., et al. (2011). Infusion of ex vivo expanded T regulatory cells in adults transplanted with umbilical cord blood: safety profile and detection kinetics. Blood *117*, 1061–1070. https://doi.org/10.1182/blood-2010-07-293795.
6. Brunstein, C.G., Miller, J.S., McKenna, D.H., Hippen, K.L., DeFor, T.E., Sumstad, D., Curtsinger, J., Verneris, M.R., MacMillan, M.L., Levine, B.L., et al. (2016). Umbilical cord blood-derived T regulatory cells to prevent GVHD: kinetics, toxicity profile, and clinical effect. Blood *127*, 1044–1051. https://doi.org/10.1182/blood-2015-06-653667.
7. Kadia, T.M., Huang, M., Pemmaraju, N., Abbas, H.A., Ly, C., Masarova, L., Yilmaz, M., Lyu, M.A., Zeng, K., Sadeghi, T., et al. (2024). Phase 1 Study of CK0801 in Treatment of Bone Marrow Failure Syndromes. NEJM Evid. *3*, EVIDoa2300362. https://doi.org/10.1056/EVIDoa2300362.
8. Lyu, M.A., Tang, X., Khoury, J.D., Raso, M.G., Huang, M., Zeng, K., Nishimoto, M., Ma, H., Sadeghi, T., Flowers, C.R., and Parmar, S. (2023). Allogeneic cord blood regulatory T cells decrease dsDNA antibody and improve albuminuria in systemic lupus erythematosus. Front. Immunol. *14*, 1217121. https://doi.org/10.3389/fimmu.2023.1217121.
9. Chow, Z., Banerjee, A., and Hickey, M.J. (2015). Controlling the fire–tissue-specific mechanisms of effector regulatory T-cell homing. Immunol. Cell Biol. *93*, 355–363. https://doi.org/10.1038/icb.2014.117.
10. Zou, L., Barnett, B., Safah, H., Larussa, V.F., Evdemon-Hogan, M., Mottram, P., Wei, S., David, O., Curiel, T.J., and Zou, W. (2004). Bone marrow is a reservoir for CD4+CD25+ regulatory T cells that traffic through CXCL12/CXCR4 signals. Cancer Res. *64*, 8451–8455. https://doi.org/10.1158/0008-5472.CAN-04-1987.
11. Elias, S., Sharma, R., Schizas, M., Valdez, I., Rampersaud, S., Park, S.M., Gonzalez-Figueroa, P., Li, Q.Z., Hoyos, B., and Rudensky, A.Y. (2022). CXCR4+ Treg cells control serum IgM levels and natural IgM autoantibody production by B-1 cells in the bone marrow. J. Exp. Med. *219*, e20220047. https://doi.org/10.1084/jem.20220047.
12. Abdelouahab, H., Zhang, Y., Wittner, M., Oishi, S., Fujii, N., Besancenot, R., Plo, I., Ribrag, V., Solary, E., Vainchenker, W., et al. (2017). CXCL12/CXCR4 pathway is activated by oncogenic JAK2 in a PI3K-dependent

manner. Oncotarget *8*, 54082–54095. https://doi.org/10.18632/oncotarget.10789.
13. Gleitz, H.F.E., Benabid, A., and Schneider, R.K. (2021). Still a burning question: the interplay between inflammation and fibrosis in myeloproliferative neoplasms. Curr. Opin. Hematol. *28*, 364–371. https://doi.org/10.1097/MOH.0000000000000669.
14. Halim, L., Romano, M., McGregor, R., Correa, I., Pavlidis, P., Grageda, N., Hoong, S.J., Yuksel, M., Jassem, W., Hannen, R.F., et al. (2017). An Atlas of Human Regulatory T Helper-like Cells Reveals Features of Th2-like Tregs that Support a Tumorigenic Environment. Cell Rep. *20*, 757–770. https://doi.org/10.1016/j.celrep.2017.06.079.
15. Bianchi, M.E., and Mezzapelle, R. (2020). The Chemokine Receptor CXCR4 in Cell Proliferation and Tissue Regeneration. Front. Immunol. *11*, 2109. https://doi.org/10.3389/fimmu.2020.02109.
16. Mora, J.R., Iwata, M., Eksteen, B., Song, S.Y., Junt, T., Senman, B., Otipoby, K.L., Yokota, A., Takeuchi, H., Ricciardi-Castagnoli, P., et al. (2006). Generation of gut-homing IgA-secreting B cells by intestinal dendritic cells. Science *314*, 1157–1160. https://doi.org/10.1126/science.1132742.
17. Sun, L., and Babushok, D.V. (2020). Secondary myelodysplastic syndrome and leukemia in acquired aplastic anemia and paroxysmal nocturnal hemoglobinuria. Blood *136*, 36–49. https://doi.org/10.1182/blood.2019000940.
18. Tan, C.L., Kuchroo, J.R., Sage, P.T., Liang, D., Francisco, L.M., Buck, J., Thaker, Y.R., Zhang, Q., McArdel, S.L., Juneja, V.R., et al. (2021). PD-1 restraint of regulatory T cell suppressive activity is critical for immune tolerance. J. Exp. Med. *218*, e20182232. https://doi.org/10.1084/jem.20182232.
19. Chapman, N.M., and Chi, H. (2014). mTOR signaling, Tregs and immune modulation. Immunotherapy *6*, 1295–1311. https://doi.org/10.2217/imt.14.84.
20. Lowther, D.E., Goods, B.A., Lucca, L.E., Lerner, B.A., Raddassi, K., van Dijk, D., Hernandez, A.L., Duan, X., Gunel, M., Coric, V., et al. (2016). PD-1 marks dysfunctional regulatory T cells in malignant gliomas. JCI Insight *1*, e85935. https://doi.org/10.1172/jci.insight.85935.
21. Kucia, M., Reca, R., Miekus, K., Wanzeck, J., Wojakowski, W., Janowska-Wieczorek, A., Ratajczak, J., and Ratajczak, M.Z. (2005). Trafficking of normal stem cells and metastasis of cancer stem cells involve similar mechanisms: pivotal role of the SDF-1-CXCR4 axis. Stem Cell. *23*, 879–894. https://doi.org/10.1634/stemcells.2004-0342.
22. Ishikawa, F., Yoshida, S., Saito, Y., Hijikata, A., Kitamura, H., Tanaka, S., Nakamura, R., Tanaka, T., Tomiyama, H., Saito, N., et al. (2007). Chemotherapy-resistant human AML stem cells home to and engraft within the bone-marrow endosteal region. Nat. Biotechnol. *25*, 1315–1321. https://doi.org/10.1038/nbt1350.
23. Dar, A., Kollet, O., and Lapidot, T. (2006). Mutual, reciprocal SDF-1/CXCR4 interactions between hematopoietic and bone marrow stromal cells regulate human stem cell migration and development in NOD/SCID chimeric mice. Exp. Hematol. *34*, 967–975. https://doi.org/10.1016/j.exphem.2006.04.002.
24. Dar, A., Goichberg, P., Shinder, V., Kalinkovich, A., Kollet, O., Netzer, N., Margalit, R., Zsak, M., Nagler, A., Hardan, I., et al. (2005). Chemokine receptor CXCR4-dependent internalization and resecretion of functional chemokine SDF-1 by bone marrow endothelial and stromal cells. Nat. Immunol. *6*, 1038–1046. https://doi.org/10.1038/ni1251.
25. Ernst, P.B., Garrison, J.C., and Thompson, L.F. (2010). Much ado about adenosine: adenosine synthesis and function in regulatory T cell biology. J. Immunol. *185*, 1993–1998. https://doi.org/10.4049/jimmunol.1000108.
26. Shevyrev, D., and Tereshchenko, V. (2019). Treg Heterogeneity, Function, and Homeostasis. Front. Immunol. *10*, 3100. https://doi.org/10.3389/fimmu.2019.03100.
27. Peiser, M., Becht, A., and Wanner, R. (2007). Antibody blocking of MHC II on human activated regulatory T cells abrogates their suppressive potential. Allergy *62*, 773–780. https://doi.org/10.1111/j.1398-9995.2007.01339.x.
28. Miragaia, R.J., Gomes, T., Chomka, A., Jardine, L., Riedel, A., Hegazy, A.N., Whibley, N., Tucci, A., Chen, X., Lindeman, I., et al. (2019). Single-Cell Transcriptomics of Regulatory T Cells Reveals Trajectories of Tissue Adaptation. Immunity *50*, 493–504.e7. https://doi.org/10.1016/j.immuni.2019.01.001.
29. Ma, X., Cao, L., Raneri, M., Wang, H., Cao, Q., Zhao, Y., Bediaga, N.G., Naselli, G., Harrison, L.C., Hawthorne, W.J., et al. (2023). Human HLA-DR+CD27+ regulatory T cells show enhanced antigen-specific suppressive function. JCI Insight *8*, e162978. https://doi.org/10.1172/jci.insight.162978.
30. Yamazaki, T., Yang, X.O., Chung, Y., Fukunaga, A., Nurieva, R., Pappu, B., Martin-Orozco, N., Kang, H.S., Ma, L., Panopoulos, A.D., et al. (2008). CCR6 regulates the migration of inflammatory and regulatory T cells. J. Immunol. *181*, 8391–8401. https://doi.org/10.4049/jimmunol.181.12.8391.
31. Kleinewietfeld, M., Puentes, F., Borsellino, G., Battistini, L., Rötzschke, O., and Falk, K. (2005). CCR6 expression defines regulatory effector/memory-like cells within the CD25(+) CD4+ T-cell subset. Blood *105*, 2877–2886. https://doi.org/10.1182/blood-2004-07-2505.
32. Jatczak-Pawlik, I., Wolinski, P., KsiĄŻek-Winiarek, D., Pietruczuk, M., and Glabinski, A. (2020). CCR6 blockade on regulatory T cells ameliorates experimental model of multiple sclerosis. Cent. Eur. J. Immunol. *45*, 256–266. https://doi.org/10.5114/ceji.2020.101241.
33. Koch, M.A., Tucker-Heard, G., Perdue, N.R., Killebrew, J.R., Urdahl, K.B., and Campbell, D.J. (2009). The transcription factor T-bet controls regulatory T cell homeostasis and function during type 1 inflammation. Nat. Immunol. *10*, 595–602. https://doi.org/10.1038/ni.1731.
34. Kitz, A., and Dominguez-Villar, M. (2017). Molecular mechanisms underlying Th1-like Treg generation and function. Cell. Mol. Life Sci. *74*, 4059–4075. https://doi.org/10.1007/s00018-017-2569-y.
35. Sakaguchi, S., Vignali, D.A.A., Rudensky, A.Y., Niec, R.E., and Waldmann, H. (2013). The plasticity and stability of regulatory T cells. Nat. Rev. Immunol. *13*, 461–467. https://doi.org/10.1038/nri3464.
36. Chaudhry, A., Samstein, R.M., Treuting, P., Liang, Y., Pils, M.C., Heinrich, J.M., Jack, R.S., Wunderlich, F.T., Brüning, J.C., Müller, W., and Rudensky, A.Y. (2011). Interleukin-10 signaling in regulatory T cells is required for suppression of Th17 cell-mediated inflammation. Immunity *34*, 566–578. https://doi.org/10.1016/j.immuni.2011.03.018.
37. Liu, B., Salgado, O.C., Singh, S., Hippen, K.L., Maynard, J.C., Burlingame, A.L., Ball, L.E., Blazar, B.R., Farrar, M.A., Hogquist, K.A., and Ruan, H.B. (2019). The lineage stability and suppressive program of regulatory T cells require protein O-GlcNAcylation. Nat. Commun. *10*, 354. https://doi.org/10.1038/s41467-019-08300-3.
38. Yao, J.C., Oetjen, K.A., Wang, T., Xu, H., Abou-Ezzi, G., Krambs, J.R., Uttarwar, S., Duncavage, E.J., and Link, D.C. (2022). TGF-beta signaling in myeloproliferative neoplasms contributes to myelofibrosis without disrupting the hematopoietic niche. J. Clin. Invest. *132*, e154092. https://doi.org/10.1172/JCI154092.
39. Marneth, A.E., and Mullally, A. (2020). Busy signal: platelet-derived growth factor activation in myelofibrosis. Haematologica *105*, 1988–1990. https://doi.org/10.3324/haematol.2020.253708.
40. Kramer, F., Dernedde, J., Mezheyeuski, A., Tauber, R., Micke, P., and Kappert, K. (2020). Platelet-derived growth factor receptor beta activation and regulation in murine myelofibrosis. Haematologica *105*, 2083–2094. https://doi.org/10.3324/haematol.2019.226332.
41. Øbro, N.F., Grinfeld, J., Belmonte, M., Irvine, M., Shepherd, M.S., Rao, T.N., Karow, A., Riedel, L.M., Harris, O.B., Baxter, E.J., et al. (2020). Longitudinal Cytokine Profiling Identifies GRO-alpha and EGF as Potential Biomarkers of Disease Progression in Essential Thrombocythemia. Hemasphere *4*, e371. https://doi.org/10.1097/HS9.0000000000000371.
42. Walz, T.M., Malm, C., Nishikawa, B.K., and Wasteson, A. (1995). Transforming growth factor-alpha (TGF-alpha) in human bone marrow: demonstration of TGF-alpha in erythroblasts and eosinophilic precursor cells and of epidermal growth factor receptors in blastlike cells of myelomonocytic origin. Blood *85*, 2385–2392.
43. Nazha, A., Khoury, J.D., Rampal, R.K., and Daver, N. (2015). Fibrogenesis in Primary Myelofibrosis: Diagnostic, Clinical, and Therapeutic Implications. Oncol. *20*, 1154–1160. https://doi.org/10.1634/theoncologist.2015-0094.
44. Desterke, C., Bilhou-Nabéra, C., Guerton, B., Martinaud, C., Tonetti, C., Clay, D., Guglielmelli, P., Vannucchi, A., Bordessoule, D., Hasselbalch, H., et al. (2011). FLT3-mediated p38-MAPK activation participates in the control of megakaryopoiesis in primary myelofibrosis. Cancer Res. *71*, 2901–2915. https://doi.org/10.1158/0008-5472.CAN-10-1731.
45. Leimkühler, N.B., and Schneider, R.K. (2019). Inflammatory bone marrow microenvironment. Hematology Am. Soc. Hematol. Educ. Program *2019*, 294–302. https://doi.org/10.1182/hematology.2019000045.
46. Rahman, M.F.U., Yang, Y., Le, B.T., Dutta, A., Posyniak, J., Faughnan, P., Sayem, M.A., Aguilera, N.S., and Mohi, G. (2022). Interleukin-1 contributes to clonal expansion and progression of bone marrow fibrosis in JAK2V617F-induced myeloproliferative neoplasm. Nat. Commun. *13*, 5347. https://doi.org/10.1038/s41467-022-32928-3.
47. Huang, H., Kim, H.J., Chang, E.J., Lee, Z.H., Hwang, S.J., Kim, H.M., Lee, Y., and Kim, H.H. (2009). IL-17 stimulates the proliferation and

differentiation of human mesenchymal stem cells: implications for bone remodeling. Cell Death Differ. *16*, 1332–1343. https://doi.org/10.1038/cdd.2009.74.

48. Li, J., Ge, M., Lu, S., Shi, J., Li, X., Wang, M., Huang, J., Shao, Y., Huang, Z., Zhang, J., et al. (2017). Pro-inflammatory effects of the Th1 chemokine CXCL10 in acquired aplastic anaemia. Cytokine *94*, 45–51. https://doi.org/10.1016/j.cyto.2017.04.010.
49. Dorner, B.G., Scheffold, A., Rolph, M.S., Huser, M.B., Kaufmann, S.H.E., Radbruch, A., Flesch, I.E.A., and Kroczek, R.A. (2002). MIP-1alpha, MIP-1beta, RANTES, and ATAC/lymphotactin function together with IFN-gamma as type 1 cytokines. Proc. Natl. Acad. Sci. USA *99*, 6181–6186. https://doi.org/10.1073/pnas.092141999.
50. Deshmane, S.L., Kremlev, S., Amini, S., and Sawaya, B.E. (2009). Monocyte chemoattractant protein-1 (MCP-1): an overview. J. Interferon Cytokine Res. *29*, 313–326. https://doi.org/10.1089/jir.2008.0027.
51. Dufour, C., Corcione, A., Svahn, J., Haupt, R., Poggi, V., Béka'ssy, A.N., Scimè, R., Pistoria, A., and Pistoia, V. (2003). TNF-alpha and IFN-gamma are overexpressed in the bone marrow of Fanconi anemia patients and TNF-alpha suppresses erythropoiesis in vitro. Blood *102*, 2053–2059. https://doi.org/10.1182/blood-2003-01-0114.
52. Gravano, D.M., Al-Kuhlani, M., Davini, D., Sanders, P.D., Manilay, J.O., and Hoyer, K.K. (2016). CD8(+) T cells drive autoimmune hematopoietic stem cell dysfunction and bone marrow failure. J. Autoimmun. *75*, 58–67. https://doi.org/10.1016/j.jaut.2016.07.007.
53. Mora, J.R., Bono, M.R., Manjunath, N., Weninger, W., Cavanagh, L.L., Rosemblatt, M., and Von Andrian, U.H. (2003). Selective imprinting of gut-homing T cells by Peyer's patch dendritic cells. Nature *424*, 88–93. https://doi.org/10.1038/nature01726.
54. Baron, U., Floess, S., Wieczorek, G., Baumann, K., Grützkau, A., Dong, J., Thiel, A., Boeld, T.J., Hoffmann, P., Edinger, M., et al. (2007). DNA demethylation in the human FOXP3 locus discriminates regulatory T cells from activated FOXP3(+) conventional T cells. Eur. J. Immunol. *37*, 2378–2389. https://doi.org/10.1002/eji.200737594.
55. Parmar, S., Robinson, S.N., Komanduri, K., St John, L., Decker, W., Xing, D., Yang, H., McMannis, J., Champlin, R., de Lima, M., et al. (2006). Ex vivo expanded umbilical cord blood T cells maintain naive phenotype and TCR diversity. Cytotherapy *8*, 149–157. https://doi.org/10.1080/14653240600620812.
56. Parmar, S., Liu, X., Tung, S.S., Robinson, S.N., Rodriguez, G., Cooper, L.J.N., Yang, H., Shah, N., Yang, H., Konopleva, M., et al. (2014). Third-party umbilical cord blood-derived regulatory T cells prevent xenogenic graft-versus-host disease. Cytotherapy *16*, 90–100. https://doi.org/10.1016/j.jcyt.2013.07.009. S1465-3249(13)00638-5.
57. Zeng, K., Huang, M., Lyu, M.A., Khoury, J.D., Ahmed, S., Patel, K.K., Dropulić, B., Reese-Koc, J., Caimi, P.F., Sadeghi, T., et al. (2023). Adjunct Therapy with T Regulatory Cells Decreases Inflammation and Preserves the Anti-Tumor Activity of CAR T Cells. Cells *12*, 1880. https://doi.org/10.3390/cells12141880.

## STAR★METHODS

### KEY RESOURCES TABLE

| REAGENT or RESOURCE | SOURCE | IDENTIFIER |
|---|---|---|
| Antibodies | | |
| Alexa Floyur532-conjugated anti-human CD3 | Invitrogen | Cat# 58-0038-42; RRID: AB_11218675 |
| BV650-conjugated anti-human CD4 | BD Biosciences | Cat# 563875; RRID: AB_2744425 |
| BV786-conjugated anti-human CD8 | BD Biosciences | Cat# 563823; RRID: AB_2687487 |
| BV421-conjugated anti-human CD25 | BD Biosciences | Cat# 562442; RRID: AB_11154578 |
| PE-conjugated anti-human CD25 | BD Biosciences | Cat# 567489; RRID: AB_2916621 |
| BUV496-conjugated anti-human CD25 | BD Biosciences | Cat# 741201; RRID: AB_741201 |
| PE-Cyaine 7-conjugated anti-human CD127 | Invitrogen | Cat# 25-1278-42; RRID: AB_1659672 |
| APC-conjugated anti-human CXCR4 | Invitrogen | Cat# 17-9999-42; RRID: AB_1724113 |
| PE-conjugated anti-human CCR7 | BD Biosciences | Cat# 566742; RRID: AB_2864275 |
| eFluor450-conjugated anti-human CD62L | Invitrogen | Cat#48-0621-82; RRID: AB_1963590 |
| BV605-conjugated anti-human CD45RA | BD Biosciences | Cat#562886; RRID: AB_2737865 |
| BV711-conjugated anti-human CD45RO | Biolegend | Cat#304236; RRID: AB_2562107 |
| BUV395-conjugated anti-human CCR6 | BD Biosciences | Cat# 743356; RRID: AB_2741448 |
| PerCP eFluor710-conjugated anti-human CCR4 | Invitrogen | Cat#46-1949-42; RRID: AB_2573725 |
| PerCP Cy5.5-conjugated anti-human CXCR3 | Biolegend | Cat# 353714; RRID: AB_10962908 |
| Alexa fLuor700-conjugated anti-human CXCR5 | Biolegend | Cat#356916; RRID: AB_2562290 |
| Alexa Fluor PE594-conjugated anti-human CD39 | Biolegend | Cat# 328232; RRID: AB_2686985 |
| APC/FIre750-conjugated anti-human CD73 | Biolegend | Cat#344036: RRID: AB_2876649 |
| PE-Cyaine 5-conjugated anti-human CD95 | Invitrogen | Cat# 15-0959-42; RRID: AB_11042290 |
| Alexa Fluor 647-conjugated anti-human HLA-DR | Biolegend | Cat#327012; RRID: AB_893570 |
| FITC-conjugated anti-human HLA-ABC | Biolegend | Cat#311404; RRID: AB_314873 |
| BUV737-conjugated anti-human PD-1 | BD Biosciences | Cat#741881; RRID: AB_2871205 |
| PE-CF594-conjugated anti-human BCL-2 | BD Biosciences | Cat#563601; RRID: AB_2738307 |
| PerCp-Cy5.5-conjugated anti-human FOXP3 | BD Biosciences | Cat# 45-5773-82; RRID: AB_914351 |
| Alexa Fluor 647-conjugated anti-human Helios | BD Biosciences | Cat# 563951; RRID: AB_2738506 |
| FITC-conjugated anti-human IL10 | Invitrogen | Cat#RHCIL1001; RRID: AB_10375444 |
| BV421-conjugated anti-human STAT5 | BD Biosciences | Cat#562984; RRID: AB_2737931 |
| BV785-conjugated anti-human T-bet | Biolegend | Cat#644835; RRID: AB_2721566 |
| APC-R7-conjugated anti-human IFNGR | BD Biosciences | Cat# 561024; RRID: AB_2033976 |
| BUV737-conjugated rat anti-human IL4 | BD Biosciences | Cat#612835; RRID: AB_2870157 |
| BV605-conjugated anti-human IL17 | Biolegend | Cat#512326; RRID: AB_2563887 |
| BUV395-conjugated anti-human GITR | BD Biosciences | Cat# 747660; RRID: AB_2744222 |
| BV786-conjugated rat anti-mouse CD45 | BD Biosciences | Cat# 564225; RRID: AB_2716861 |

### EXPERIMENTAL MODEL AND STUDY PARTICIPANT DETAILS

#### *In vivo* xenogeneic homing mouse model

Female non-obese diabetic (NOD)-immunodeficient (SCID) IL-2Rγ-/- (NSG) mice at 5 weeks of age were acquired from Jackson Laboratory (Farmington, CT). All animal experiments were carried out in accordance with the MDACC Institutional Animal Care and Use Committees. Expanding human $Treg^{control}$ and $Treg^{CXCR4}$ cells were obtained by the Cellenkos® Inc (Houston, TX, USA) and incubated with Cell Trace Violet (CTV) cell proliferation kit (Life Technologies Corp., Oregon, USA) as per manufacturers' instruction. $1x10^7$ cells of CTV labeled

$Treg^{control}$ or $Treg^{CXCR4}$ cells were injected into tailvein (t.v.) of NSG mice. At 12 hours and 24 hours post infusion, mouse peripheral blood mononuclear cells (PBMCs), hepatocytes, splenocytes and BM cells were harvested to detect CTV-labeled cells using BD Fortessa X-20 and Cytek Aurora. To determine the homing index, the ratio of frequency of $CTV^+$ cells in the positive group ($Treg^{CXCR4}$) to the number of $CTV^+$ cells in the control group ($Treg^{control}$) was calculated.[53]

To prepare a single-cell suspensions, mouse peripheral blood was drawn into ethylenediaminetetraacetic acid (EDTA)-coated tubes, and for tissue samples, fresh liver and spleen were processed by mashing and filtering through a 40-μm cell strainer. BM cells were harvested by cutting both ends of the long bones (femur) of the hind limbs and flushing them with FACS buffer (PBS, 2%FCS, 2 mM EDTA; Lonza). Red blood cells were removed using 1x RBC lysis buffer (Miltenyi Biotec, Gladbach, Germany). All cells were resuspended in FACS buffer (Lonza, Walkersville, MD, USA) for tallying and immunolabeling.

### Bone marrow inflammation xenograft model

Five-week-old female NOD-SCID IL-2Rγ-/- (NSG) mice (The Jackson Laboratory, Bar Harbor, ME, USA) were subjected to 1.5 Gy irradiation followed by t.v. injection of $10\times10^6$ human PBMCs. In the treatment arm $10\times10^6$ $Treg^{CXCR4}$ cells injected by t.v. on days 1, 8, 15, 22, and 29. On day 30, harvested bone marrow samples from mouse femur were fixed with 10% buffered formalin and embedded in paraffin for processing into 5-μm tissue sections. Deparaffinized and rehydrated tissue sections were stained using anti-CD8, anti-TNF-α, anti-IFN-γ, and DAPI, and imaged on the Leica DMi8. Immunofluorescent images were exported using LAS X (Leica Microsystems, Wetzlar, Germany).

### Institutional approval for animal studies

Animal procedures were performed according to an approved protocol by MD.

Anderson Cancer Center's Institutional Animal Care and Use Committe.

## METHOD DETAILS

### UCB Treg cells, and $Treg^{CXCR4}$ cells isolation and *in vitro* expansion

UCB units were obtained from The University of Texas MD Anderson Cancer Center Cord Blood Bank after Institutional Review Board (IRB) approval. Using magnetic enrichment UCB Tregs (defined as $CD4^+CD25^{hi}CD127^{lo}$) were isolated based on $CD25^{hi}$ cell surface expression.[1,8] At day 3 or 4 of culture, Tregs were harvested and labeled with CD184 (CXCR4)-APC and Anti-APC Microbeads kit (CD184 MicroBead Kit, Miltenyi Biotec, Gladbach, Germany) and were positively enriched by CXCR4-postive magnetic cell sorting and cultured for a total of 14 days.

### Flow cytometry

Flow cytometry was performed to determine the phenotype of three distinct cell populations, i) pre-selection $Treg^{control}$, ii) post-enrichment ($Treg^{CXCR4}$), and iii) negative flow through ($Treg^{CXCR4neg}$) populations using a Cytek Aurora flow cytometer system. Three different marker panels were created with 20 colors, 15 colors, and 14 colors (Table S1). Cells from the first and second panels were stained with cell surface markers, while cells from the third and fourth panels were fixed and permeabilized for intracellular staining, using the Foxp3/Transcription Factor Fixation/Permeabilization Staining Buffer Set (ThermoFisher Scientific, Waltham, MA). Dead cells were excluded using a fixable viability dye (Invitrogen, Waltham, MA), and the FCS files were analyzed using FlowJo (Ashland, OR) and Cytobank software (Santa Clara, CA).

### viSNE analysis

The FCS files generated from the flow cytometer were analyzed using software programs such as FlowJo (Ashland, OR) and Cytobank 9.0 (Santa Clara, CA) to create viSNE maps. The viSNE maps were constructed by running the algorithm for 1000-7500 iterations using arbitrary seed and tSNE parameters (perplexity=30). This enabled the projection of the high-dimensional data into two dimensions, tSNE1 and tSNE2, which facilitated the visualization of the phenotypic heterogeneity of $Treg^{control}$ and $Treg^{CXCR4}$ subsets.

### DNA methylation analysis

FoxP3 Treg-specific demethylation region (TSDR) methylation analysis of $Treg^{CXCR4}$ or $Treg^{control}$ cells was performed using deep amplicon bisulfite sequencing.[54–56]

### IL-10 secretion assay

Human IL-10 levels were quantified in the cell culture supernatants using IL10 human ELISA kit (BMS215-2, ThermoFisher Scientific, Waltham, MA) as per manufacturer's instructions. Samples, standards, and controls were added to wells pre-coated with anti-human IL-10 antibody, incubated with a biotinylated antibody at 37°C for 2 hours, followed by washes and an additional incubation with Streptavidin-HRP. Tetramethylbenzidine substrate was then used to develop color, indicative of IL-10 concentration. The reaction was halted with an acidic stop solution, and the optical density was measured at 450 nm using a BioTek Epoch plate reader. Data analysis was conducted using appropriate software, and quality control was maintained through replicates and standard controls.

### Cell suppression assay

Functional ability of $Treg^{CXCR4}$ or $Treg^{control}$ cells to suppress proliferating $CD4^{+}25^{-}$ conventional T cells (Tcon) was quantified using the method of cell suppression assay, where different ratios of Treg:Tcon were examined.[1,8,57]

### Migration assay

The speed of egress of the $Treg^{CXCR4}$ vs. $Treg^{control}$ towards the chemoattractant CXCL12/SDF1α[8] was analyzed using Transwell™ migration assay [9], where chemotaxis was performed using a 24-well Boyden chamber with a 5.0 μm pore size polyvinyl pyrrolidone–free polycarbonate membrane (Corning, NY, USA). 100 ul volume of $Treg^{CXCR4}$ or $Treg^{control}$ cells, were added at a concentration of 0.5 x $10^6$ cells/mL, to the upper chamber. Simultaneously, CXCL12/SDF1α at a concentration of 300 ng/mL was introduced to the lower chamber in serum-free medium. Migration was allowed over various time points in humidified chambers at 37°C, both with and without the CXCR4 antagonist AMD3100 at a concentration of 6 μg/mL. Non-migrating Tregs located on the top of the insert were removed using a cotton swab. Subsequently, the Tregs on the inserts were fixed with 70% ethanol for 10 minutes, air-dried for an additional 10 minutes, and stained with 0.1% crystal violet. The Transwell inserts were then mounted onto slides for imaging using a microscope. The total number of cells in each image was counted for analysis.

### *In* vivo phenotype analysis by flow cytometry

Single cell suspension from PBMCs, hepatocytes, splenocytes and BM cells were stained using CTV proliferation kit, and fluorescent antibodies as shown in Table S1. Dead cells were excluded using fixable viability dye (Invitrogen, Waltham, MA). Anti-CXCL12 antibody used for *in vivo* staining showed cross species reactivity for human and mouse. Multicolor flow cytometry data acquisition was done with BD LSR Fortessa and Cytek Aurora and the FCS files were analyzed using FlowJo (Ashland, OR) and Cytobank software (Santa Clara, CA). Of $CTV^{+}$ human $Treg^{control}$ and $Treg^{CXCR4}$ cells, $CD4^{+}$ and $CD25^{+}$ co-expression was identified as Tregs. Among the human Treg cells (hTreg), $CD45RA^{+}$ and $CCR7^{+}$ were commonly used markers to distinguish resting Treg cells (rTreg), memory Treg cells (mTreg), and activated Treg cells (aTreg) in BM. In addition, CD45RO and CD62L markers could distinguish between resting Treg cells (rTreg), memory Treg cells (mTreg), and activated Treg cells (aTreg) in the spleen.

### Cytokine analysis

Plasma samples, collected from the EDTA-treated murine PB, were analyzed for systemic inflammation using a human cytokine 48-plex Discovery assay kit and TGFβ 3-Plex Discovery assay kit (Eve Technologies, Calgary, Alberta, Canada).

### Bone marrow immunostaining

Bone marrow samples collected from mouse femur were stained using anti-CD8 (BD Biosciences, Franklin Lakes, NJ), anti-TNF-α (Cell Signaling Technology, Danvers, MA), anti-IFN-γ (Bethyl laboratories, Montgomery, TX), and DAPI (4′,6-Diamidino-2-Phenylindole) (Thermo Scientific, Waltham, MA), and imaged on the Leica DMi8 (Wetzlar, Germany). The immunofluorescence analysis was conducted in a blinded fashion, with the assistance of Image J software.

### Interferon-γ ELISA

EDTA-treated plasma samples were analysed for inflammation using a human IFN-γ ELISA kit (ThermoFisher Scientific, Waltham, MA) as per manufacturer's instructions. Samples, standards, and controls were added to wells pre-coated with anti-human IFN-γ antibody, incubated with a biotinylated antibody at 37°C for 1.5 hours, followed by washes and an additional incubation with Streptavidin-HRP. TMB substrate was then used to develop color, indicative of IFN-γ concentration. The reaction was halted with an acidic stop solution, and the optical density was measured at 450 nm using a BIoTek Epoch plate reader. Data analysis was conducted using appropriate software, and quality control was maintained through replicates and standard controls.

## QUANTIFICATION AND STATISTICAL ANALYSIS

Statistical analysis was performed using Prism Version 9 software (GraphPad Software, La Jolla, CA). Statistical significance was calculated by *P* value using unpaired t-test, one-way ANOVA and two-way ANOVA. $P$ value$<0.05$ was considered statistically significant.